Lattice deformation in epitaxial Fe_3O_4 films on MgO substrates studied by polarized Raman spectroscopy*

Yang Yang(杨洋)[1,†], Qiang Zhang(张强)[2], Wenbo Mi(米文博)[3], and Xixiang Zhang(张西祥)[2]

[1] *Beijing National Laboratory for Condensed Matter Physics, Institute of Physics, Chinese Academy of Sciences, Beijing* 100190, *China*
[2] *PSE Division, King Abdullah University of Science and Technology (KAUST), Thuwal* 23955-6900, *Kingdom of Saudi Arabia*
[3] *Tianjin Key Laboratory of Low Dimensional Materials Physics and Preparation Technology, School of Science, Tianjin University, Tianjin* 300354, *China*

(Received 2 April 2020; revised manuscript received 12 May 2020; accepted manuscript online 25 May 2020)

The lattice structures of epitaxial Fe_3O_4 films deposited on MgO were studied systematically using polarized Raman spectroscopy as a function of film thickness, where interesting phenomena were observed. Firstly, the spectral conflict to the Raman selection rules (RSRs) was observed under cross-sectional configuration, which can be attributed to the tetragonal deformation in the growth direction due to the lattice mismatch between Fe_3O_4 and MgO. Secondly, the blue shift and broadening of Raman peaks evidenced the decrease of the tensile strain in Fe_3O_4 films with decreasing thickness. Thirdly, distinct from the other Raman modes, the lowest T_{2g} mode exhibited asymmetric lineshape, which can be interpreted using the spatial correlation model. The increased correlation length introduced in the model can well explain the enhanced peak asymmetry feature with decreasing thickness. These results provide useful information for understanding the lattice structure of epitaxial Fe_3O_4 film.

Keywords: polarized Raman scattering, Fe_3O_4 film, tetragonal deformation, spatial correlation model

PACS: 33.20.Fb, 68.55.–a, 74.62.Dh **DOI:** 10.1088/1674-1056/ab9615

1. Introduction

Iron oxide magnetite (Fe_3O_4), a half-metallic ferromagnet with large spin polarization and high Curie temperature of 858 K, has attracted much attention owning to its intriguing physical properties and potential applications in spintronic devices.[1–6] The further applications on devices closely rely on the physical properties of Fe_3O_4 films that depend on the type of substrates, thickness and deposition conditions. As we know, epitaxial Fe_3O_4 films have been grown on a variety of single crystal substrates, e.g., MgO, α-Al_2O_3, ZnO, Si, and GaAs, using different methods such as molecular beam epitaxy (MBE), sputtering, and pulse laser deposition (PLD).[3,7–9] Among the substrates mentioned above, MgO is one of the most frequently used because it has a nearly perfect lattice match with Fe_3O_4. The lattice constant of MgO is 4.213 Å, which is nearly the half of Fe_3O_4 (8.3967 Å). Although the lattice mismatch in Fe_3O_4 films on MgO (Fe_3O_4/MgO) is only +0.3%, the prominent changes took place in the magnetic and electronic properties of Fe_3O_4/MgO films due to the tensile strain imposed by MgO substrate.[10,11] It has been already reported that the magnetic properties of Fe_3O_4 films change significantly with the decreasing thickness, which is closely related with the existence of antiphase boundaries (APBs).[12–14] Revealing the strain effects from substrates and the changes of microstructure with thickness would provide useful information for understanding the magnetic properties of Fe_3O_4 films.

Raman spectroscopy is a powerful tool to probe the microstructure of thin films and its relationship with other physical properties of oxides.[15,16] In past decades, Raman spectroscopy has been widely employed to study the structure of Fe_3O_4 films.[8,9,17] Tiwari *et al.* have demonstrated that Raman spectroscopy is a tool to evaluate the APBs in Fe_3O_4 films.[9] Kumar *et al.* have employed Raman spectroscopy to study the spin-phonon coupling in Fe_3O_4 films at Verwey temperature.[18] However, most researches were carried using non-polarized Raman spectroscopy, while polarized Raman study of Fe_3O_4/MgO was rarely reported. With the help of polarized Raman scattering, the symmetry of Raman peaks can be assigned, and the crystallinity and orientation of film can be identified. What is more, the overlapped Raman peaks can be isolated, promising feasible peak fitting and further analysis.

In this work, Fe_3O_4 films were studied systematically as a function of film thickness by polarized Raman spectroscopy. Discrepancy to Raman selection rules (RSRs) observed in the cross-sectional geometry was attributed to the tetragonal deformation in the growth direction due to the lattice mismatch between Fe_3O_4 and MgO. Raman peaks were fitted with different numerical functions and a deeper insight into thickness effects on the structure of Fe_3O_4 films was obtained.

*Project supported by the National Key Research and Development Program of China (Grant No. 2018YFB0703500) and the National Natural Science Foundation of China (Grant No. 11704401).

†Corresponding author. E-mail: yang.yang@iphy.ac.cn

2. Experimental details

Epitaxial Fe_3O_4 films were deposited on MgO single crystal substrates using reactive magnetron sputtering. The details of deposition were reported elsewhere.[19] In this work, Fe_3O_4 films with thicknesses of 27 nm, 50 nm, 85 nm, 170 nm, 217 nm are used for the Raman study. The epitaxial properties of Fe_3O_4 films have been demonstrated using θ–2θ and Φ-scan x-ray diffraction (XRD) experiments. Raman spectra were collected under backscattering geometry using a confocal micro-Raman spectrometer (Horiba/Jobin Yvon Aramis) with a 473 nm laser source. The laser power on the film surface was less than 0.5 mW to prevent laser-induced heating effect on films. Two types of backscattering configurations, including normal and cross-sectional scattering configurations were employed in the Raman measurements. The schematic diagraphs of these two Raman measurement configurations are shown in Fig. 1, in which the X, Y and Z axes were the laboratory coordinates. The x and y axes of the Fe_3O_4 film were along the [100] and [010] directions of the MgO substrate, while the z axis was the growth direction of the film. In the normal scattering configuration as illustrated in Fig. 1(a), the x, y and z axes of films parallel respectively with the X, Y and Z axes. On the other hand, in the cross-sectional scattering configuration, the x, y and z axes of films are respectively along the Z, Y and X axes. As displayed in Fig. 1(b), the incident light propagates along the Z axis, which corresponds to the x axis of Fe_3O_4 film. Thus the incident polarization (P_i) parallel with the z axis, and the scattered polarization can be along the y (or z) axes. Cross-sectional Raman scattering can provide more information about the stress distribution, domain structure and the crystalline orientation of thin films.[20–22]

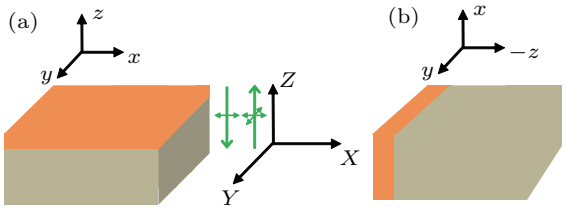

Fig. 1. Schematic drafts for (a) normal and (b) cross-sectional scattering configurations. The polarization direction of incident laser is along the X axis, while the polarization direction of scattered is along the X and Y axes for parallel (VV) and crossed (VH) scattering geometries, respectively.

3. Results and discussion

Bulk Fe_3O_4 has a cubic inverse spinel structure with space group O_h^7 ($Fd3m$), which gives rise to five Raman-active modes, $\Gamma_R = A_{1g} + E_g + 3T_{2g}$. Normally, only four peaks are observed in the Raman spectra of Fe_3O_4, as revealed in the previous studies.[8,9,17] Figure 2 displays the polarized Raman spectra of the 217-nm-thick Fe_3O_4 film collected in different scattering configurations. According to the RSRs,[23] A_{1g} and E_g modes only appear in the VV scattering geometry under the normal scattering configuration, in which P_i is along the X axis as shown in Fig. 1(a), while the T_{2g} modes show up in the VH scattering geometry. In Fig. 2(a), the Raman modes comply with the RSRs in the normal backscattering configuration. The peaks around 307 cm^{-1} and 665 cm^{-1} are assigned as the E_g and A_{1g} modes, respectively, while the peaks at 193 cm^{-1} and 535 cm^{-1} are attributed to the T_{2g} modes.[17,18,22] The Raman spectra of other thinner films share the similar polarization dependences. The good agreement between our results and RSRs suggests the highly epitaxial characteristics of Fe_3O_4 films. A very weak peak can be seen at the A_{1g} position in the VH geometry, which can be attributed to the lattice defects in the Fe_3O_4 film. Although Fe_3O_4 films were epitaxially grown, small amount of defects, such as dislocations and vacancies, cannot be excluded. It has been demonstrated by many researchers that the antiphase boundaries (APBs) is the main lattice defects that play a key role in the anomaly properties of epitaxial Fe_3O_4 films.[11,24,25] APBs are related to the lattice relaxation, formed at the junction of neighboring grains.[13,26]

In order to further study the microstructure in Fe_3O_4 films, the cross-sectional Raman scattering was carried out. In Fig. 2(c), the remarkable spectral features are observed when P_i parallels with the z axis. The $T_{2g}^{(3)}$ mode appears in the VV geometry which is in contract with the results obtained in the normal Raman scattering configuration. Furthermore, the polarized spectra resemble the features of the normal scattering configuration as the incident polarization is along the y axis (not shown here). The A_{1g} and E_g modes appear in the VV geometry, while the T_{2g} modes are observed in the VH geometry. Such spectral divergence between Figs. 2(a) and 2(c) cannot be attributed to the lattice defects in the films. If the leakage of $T_{2g}^{(3)}$ mode comes from lattice defects, $T_{2g}^{(3)}$ mode should be seen in the VV geometry all the time when the incident polarization parallels with the three axes of the film. However, it only turns out when the incident polarization parallels with z axis. As discussed previously, the crystalline axis $a = b > c$ in Fe_3O_4 films on MgO substrates. The in-plane axes are equal, so the polarized Raman spectra in the normal scattering configuration are identical while rotating the incident polarization from the x axis to the y axis. In contrast, the out-of-plane axis is compressed and shorter than the in-plane axes, giving rise to a tetragonal deformation in Fe_3O_4 films. As the lattice constant of Fe_3O_4 is slightly smaller than the double of the MgO lattice constant, the in-plane axes of Fe_3O_4 films are elongated in two directions due to the tensile stress in the film. The tetragonal deformation not only leads to the elongated in-plane axes, but also can induce the lattice dislocations in the out-of-plane axis in order to release internal stress in the film. The orientation of the crystalline

axis for the Fe_3O_4 film is not strictly along the $\langle 100 \rangle$ directions of the MgO substrate due to the existence of APBs.[13] Luysberg *et al.* have demonstrated that the presence of APBs are associated with the formation of misfit dislocations with partial Burgers vectors.[27] As demonstrated by the selected-area electron diffraction (SAED) patterns, the charge ordering of B-site Fe atoms exists in the epitaxial Fe_3O_4 films.[19] The $T_{2g}^{(3)}$ mode originates from the asymmetric bends of oxygen ions with respect to Fe ions, so that it is sensitive to the strain deformation along the crystalline axes.[28] The tetragonal deformation in the film would contribute to the conflicts to RSRs for the $T_{2g}^{(3)}$ mode.[29] As presented in Fig. 2(b), the $T_{2g}^{(3)}$ mode arises in the VV geometry after rotating the polarization by 45° under the normal incident configuration. According to the RSRs, the $T_{2g}^{(3)}$ mode is not zero when the incident and scattered polarizations are parallel to the [110] direction. The VV spectra in the cross-sectional configuration (Fig. 2(c)) exhibits the obvious similarity to the VV spectra under 45° polarization geometry in Fig. 2(b), suggesting the existence of nano-sized areas in which the lattice dislocations are along the $\langle 110 \rangle$ directions. Therefore, the presence of $T_{2g}^{(3)}$ mode in the VV spectra in the cross-sectional configuration undoubtedly demonstrated the existence of APBs.

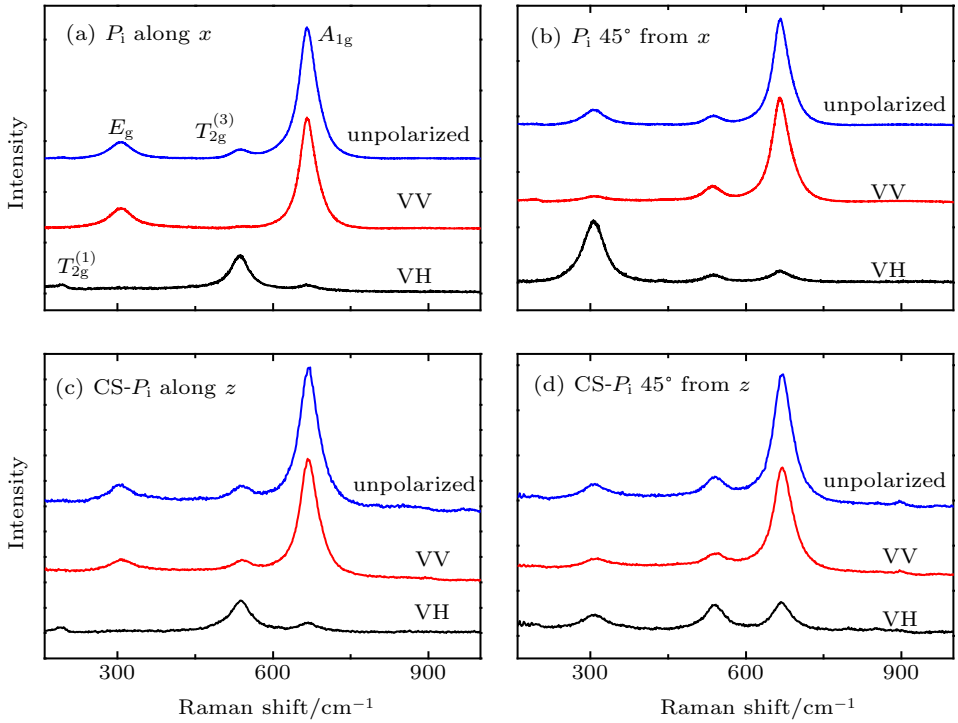

Fig. 2. Polarized Raman spectra of the Fe_3O_4 film of 217 nm obtained in the normal [(a) and (b)] and cross-sectional [(c) and (d)] scattering configuration.

In order to get a clear insight into the evolution of Raman peaks as a function of film thickness, the Raman spectra were deconvoluted using the Lorentz/Gaussian mixed function. Figures 3(a)–3(c) show the thickness-dependent peak positions of E_g, $T_{2g}^{(3)}$ and A_{1g} modes. Taking the A_{1g} mode as an example, it shifts from 671.7 cm^{-1} to 668 cm^{-1} quickly when the film thickness increases from 27 nm to 85 nm (6.4×10^{-2} cm^{-1}/nm). The similar phenomenon was observed by Tiwari *et al.* in the Fe_3O_4 films thinner than 150 nm.[9] Then, the peak position of A_{1g} mode varies slowly, with a rate of 5.8×10^{-3} cm^{-1}/nm, for a thicker film, as exhibited in Fig. 3(c). The other two peaks shift following the same trace as that of the A_{1g} mode. As presented in Figs. 3(d)–3(f), similar to the peak position, bandwidth decreases while film thickness increases from 27 nm to 85 nm, then keeps at a constant for thicker films. As we know, bandwidth is the reciprocal of phonon lifetime, which decreases while lattice defects increase, so that the broadening of Raman peaks is associated with the increasing defects in the lattice.[30,31] More lattice defects emerge as a result of the increasing density of APBs while the film thickness is decreasing.[27,29,32] Thus, the broadening of Raman peaks of Fe_3O_4 films can be attributed to the increasing APBs when the film thickness decreases. It is accepted that the lattice relaxation takes place to release internal stress while the film thickness increases.[27,29] At the same time, the grain size in the film becomes larger as a result of decreasing APBs.[13] From the Raman spectra, one can see the improvement of Raman signal, such as bandwidth shrinking and frequency softening, as presented in Fig. 3.

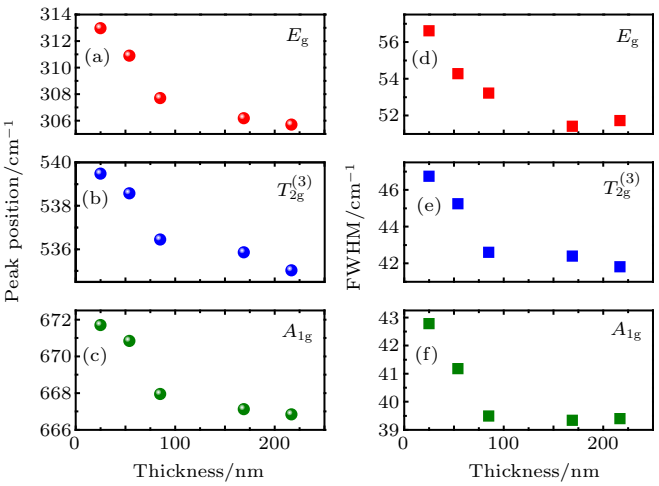

Fig. 3. Thickness-dependent peak position and bandwidth (FWHM) of E_g, $T_{2g}^{(2)}$ and A_{1g} modes.

Taking a close look at the fitting curves of Raman peaks, it is interesting to find that the lineshapes of Raman peaks are different. One can see that the $T_{2g}^{(1)}$ mode exhibits an asymmetric lineshape with a tail at low frequency, as presented in Fig. 4(a). In sharp contrast, as shown in Figs. 4(b)–4(d), the E_g, $T_{2g}^{(3)}$ and A_{1g} modes show the symmetric lineshape, which can be well fitted by the Lorentz function, implying the good crystalline quality of Fe_3O_4 films. The asymmetric lineshape comes from the lattice disorder effects, which has been observed in some oxides and semiconductor films.[33–35] In the ideal single crystal, only phonons near the center of Brillouin zone ($q \sim 0$) contributed to the Raman spectrum. On the other hand, the disorders in the film result in the breaking of the translational symmetry, leading to the contribution of $q \neq 0$ phonons to Raman lineshape, which is the so-called finite-size effect. Since the Fe_3O_4 films in our hand are highly oriented, the lattice defects are low. As we know, the defects in Fe_3O_4 films mainly from the location shift of Fe ions.[36] This kind of defects mainly affects the low frequency Raman peaks, so that the $T_{2g}^{(1)}$ mode exhibits an asymmetric lineshape. Furthermore, these high-frequency E_g, $T_{2g}^{(2)}$ and A_{1g} modes originating from Fe–O vibrations keep the symmetric Lorentz lineshape. The asymmetric lineshape of Raman modes can be described by a spatial correlation model. The assumption of a Gaussian factor $\exp(-q^2L^2)$, where L is the diameter of the correlation region, is employed in the spectra fitting of mode $T_{2g}^{(1)}$.[33–35]

The Raman intensity $I(\omega)$ at a frequency ω can be written as

$$I(\omega) \sim \int_0^1 \exp\left(-\frac{q^2L^2}{4}\right) \frac{4\pi q^2 \mathrm{d}^3 q}{[\omega - \omega(q)]^2 + (\frac{\gamma(q)}{2})^2},$$

where q is expressed in units of $2\pi/a$, and L is in units of a with a being the lattice constant. L is the correlation length, which reflects the degree of disorder in the film; $\gamma(q)$ is the linewidth of phonon, which is independent of q. For the dispersion curve $\omega(q)$, it can be expressed as $\omega(q) = \omega_0 - Bq^2$,[34] with $\omega_0 = 196$ cm^{-1} and $B = 29.9$ cm^{-1}.

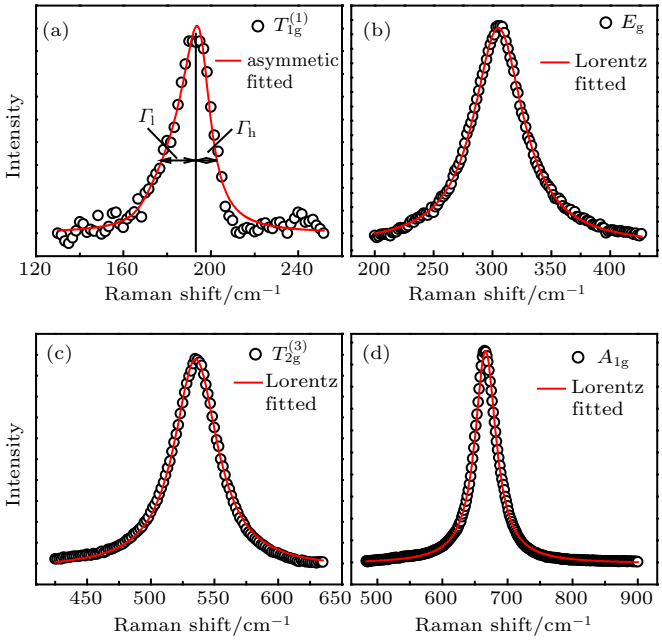

Fig. 4. Different Raman modes and their corresponding numerically fitted curves. Black circles represent the experimental results, the red lines are the fitting results.

As shown in Fig. 5(a), the bandwidth increases while film thickness is decreasing, especially for the films thinner than 100 nm. The broadened bandwidth clearly evidences more lattice defects in thinner Fe_3O_4 films. Interestingly, one can see from Fig. 5(b) that L increases with decreasing thickness, following the same trace of bandwidth. As we know, L is the correlation length, which can be used to represent the grain size in the film.[33–35] The results shown in Fig. 5(b) suggest that the correlation length (or grain size) increases with the decreasing film thickness. It has been reported that the asymmetry feature becomes smaller with the increasing correlation length. The asymmetry of $T_{2g}^{(1)}$ is calculated using the ratio of half-widths at half maximum on low- and high-frequency sides (Γ_l/Γ_h). As shown in the inset of Fig. 5(b), the asymmetric ratio of $T_{2g}^{(1)}$ becomes smaller in a thinner film, which agrees well with the prediction from the variation of L. It has been demonstrated that the density of APBs in a thin Fe_3O_4 film is higher than that in a thick Fe_3O_4 film. Consequently, the grain size in a thinner Fe_3O_4 film is thought to be smaller. However, as shown in Fig. 5(b), grain size increases in the thin Fe_3O_4 film. As we know, L is physically the correlation length for Raman phonons, in which phonons can propagate freely. Our results suggest that APBs are just a kind of lattice defects rather than crystalline boundaries, at least phonons take the adjacent antiphase areas as a whole for propagation.

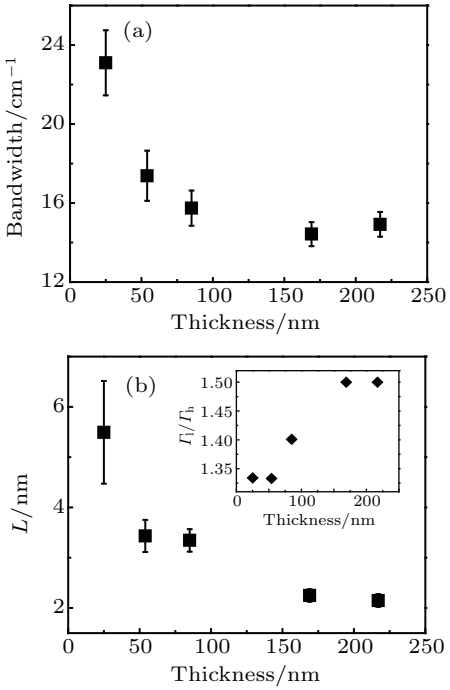

Fig. 5. (a) bandwidth and (b) correlation length for $T_{2g}^{(1)}$ mode as a function of thickness. The inset shows the thickness dependence of the ratio of half-widths at half maximum on low- and high-frequency sides (Γ_l/Γ_h).

4. Conclusions

In this work, polarized Raman spectroscopy has been employed to investigate the microstructure of Fe_3O_4 films as a function of film thickness. The Raman spectra in the cross-sectional configuration clearly imply the tetragonal deformation in the growth direction due to the lattice mismatch between Fe_3O_4 films and MgO substrates. The Raman peaks shifting to a higher frequency indicates the decrease of tensile strain with decreasing film thickness, while the broadened peaks imply the increasing lattice defects due to the increasing density of APBs. Moreover, the lowest T_{2g} mode exhibits an asymmetric lineshape, which can be used to monitor the grain size in the Fe_3O_4 film. Our results provide a deeper insight into the lattice structure of Fe_3O_4 films on MgO substrates, which are expected to be helpful for preparation of Fe_3O_4 films and further applications in spintronic devices.

References

[1] Yanase A and Hamada N 1999 *J. Phys. Soc. Jpn.* **68** 1607
[2] Dedkov Y S, Rudiger U and Guntherodt G 2002 *Phys. Rev. B* **65** 064417
[3] Li Y, Han W, Swartz A G, Pi K, Wong J J I, Mack S, Awschalom D D and Kawakami R K 2010 *Phys. Rev. Lett.* **105** 167203
[4] Wolf S A, Awschalom D D, Buhrman R A, Daughton J M, Von S, Roukes M L, Chtchelkanova A Y and Treger D M 2001 *Science* **294** 1488
[5] Zutic I, Fabian J and Das S 2004 *Rev. Mod. Phys.* **76** 323
[6] Schmidt G 2005 *J. Phys. D: Appl. Phys.* **38** R107
[7] Paul M, Kufer D, Müller A, Brück S, Goering E, Kamp M, Verbeeck J, Tian H, Van G, Ingle N J C, Sing M and Claessen R 2011 *Appl. Phys. Lett.* **98** 012512
[8] Phase D M, Tiwari S, Prakash R, Dubey A, Sathe V G and Choudhary R J 2006 *J. Appl. Phys.* **100** 123703
[9] Tiwari S, Phase D M and Choudhary R J 2008 *Appl. Phys. Lett.* **93** 234108
[10] Kleint C A, Semmelhack H C, Lorentz M and Krause M K 1995 *J. Magn. Magn. Mater.* **140-144** 725
[11] Chen Y X, Chen C, Zhou W L, Wang Z J, Tang J, Wang D X and Daughton J M 2004 *J. Appl. Phys.* **95** 7282
[12] Liu H, Jiang E Y, Bai H L, Zheng R K and Zhang X X 2003 *J. Phys. D: Appl. Phys.* **36** 2950
[13] Eerenstein W, Palstra T T M, Hibma T and Celotto S 2002 *Phys. Rev. B* **66** 201101(R)
[14] Ramos A V, Moussy J B, Guittet M J, Bataille A M, Gautier-Soyer M, Viret M, Gatel C, Bayle-Guillemaud P and Snoeck E 2006 *J. Appl. Phys.* **100** 103902
[15] Yang Y, Zhang Q, Zhang B, Mi W B, Chen L, Li L, Zhao C, Diallo E M and Zhang X X 2012 *Appl. Surf. Sci.* **258** 4532
[16] Wang S S, Li F, Wu H, Zhang Y, Muhammad S, Zhao P, Le X Y, Xiao ZiS, Jiang L X), Ou X D and Ouyang X P 2019 *Chin. Phys. B* **28** 027401
[17] Zhang J, Tan P H, Zhao W J, Lu J and Zhao J H 2011 *J. Raman. Spectrosc.* **42** 1388
[18] Kumar A, Chaudhary S, Pandya D K and Sharma S K 2014 *Phys. Rev. B* **90** 024302
[19] Mi W B, Guo Z B, Wang Q X, Yang Y and Bai H 2013 *Scr. Mater.* **68** 972
[20] Bartasyte A, Margueron S, Kreisel J, Bourson P, Chaix-Pluchery O, Rapenne-Homand L, Santiso J, Jimenez C, Abrutis A, Weiss F and Fontana M D 2009 *Phys. Rev. B* **79** 104104
[21] Lin H C, Feng Z C, Chen M S, Shen Z X, Ferguson I T and Lu W 2009 *J. Appl. Phys.* **105** 036102
[22] Pezzotti G, Sueoka H, Porporati A A, Manghnani M and Zhu W L 2011 *J. Appl. Phys.* **110** 013527
[23] Loudon R 1964 *Adv. Phys.* **13** 423
[24] Margulies D T, Parker F T, Rudee M L, Spada F E, Chapman J N, Aitchison P R and Berkowitz A E 1997 *Phys. Rev. Lett.* **79** 5162
[25] Coey J M D, Berkowitz A E, Balcells L I, Putris F F and Parker F T 1998 *Appl. Phys. Lett.* **72** 734
[26] Hong J P, Lee S B, Jung Y W, Lee J H, Yoon K S, Kim K W, Kim C O and Lee C H 2003 *Appl. Phys. Lett.* **83** 1590
[27] Luysberg M, Sofin R G S, Arora S K and Shvets I V 2009 *Phys. Rev. B* **80** 024111
[28] Shebanova O N and Lazor P 2003 *J. Solid State Chem.* **174** 424
[29] Iliev M N, Mazumdar D, Ma J X, Gupta A, Rigato F and Fontcuberta J 2011 *Phys. Rev. B* **83** 014108
[30] Kitajima M 1997 *Critical Reviews in Solid State and Materials Sciences* **22** 275
[31] Bartasyte A, Chaix-Pluchery O, Kreisel J, Jimenez C, Weiss F, Abrutis A, Saltyte Z and Boudard M 2008 *J. Appl. Phys.* **103** 014103
[32] Bollero A, Ziese M, Höhne R, Semmelhack H C, Köhler U, Setzer A and Esquinazi P 2005 *J. Magn. Magn. Mater.* **285** 279
[33] Yoshikawa M, Mori Y, Maegawa M, Katagiri G, Ishida H and Ishitani A 1993 *Appl. Phys. Lett.* **62** 3114
[34] Sui Z F, Leong P P, Herman I P, Higashi G S and Temkin H 1992 *Appl. Phys. Lett.* **60** 2086
[35] Lin L Y, Chang C W, Chen W H, Chen Y F, Guo S P and Tamargo M C 2004 *Phys. Rev. B* **69** 075204
[36] Chamritski I and Burns G 2005 *J. Phys. Chem. B* **109** 4965